THE IMPACT OF SLOPE VARIABILITY ON THE MODELING OF MARTIAN LAVA FLOWS. Frances P. Russo[1], Ian T.W. Flynn[1], and Michael S. Ramsey[1], [1]Department of Geology and Environmental Science, University of Pittsburgh, Pittsburgh, PA 15260. fpr4@pitt.edu

Introduction: Prior morphological studies of lava flows in the Tharsis region of Mars have used different models to determine viscosity, emplacement time, effusion rate, and other rheologic parameters [e.g., 1-4]. Investigation of channelized lava flows have made use of a variety of modeling techniques [5-8]. A frequently used method is that of a "standard rheologic approach", which has been applied to flows throughout the Tharsis volcanic province [5,6].

One assumption made in this approach is that of a constant average slope, which can have a measurable impact on the final results [9,10]. Our study measured the individual slopes of eight lava flows throughout the Tharsis volcanic province, and examines how the minimum and maximum slope values impact the standard rheologic approach results.

Mars Dataset: Channelized flows were investigated in this study. Each flow length was mapped down the center of its central channel using data from the Context Camera (CTX) (~6 m/pixel) (Fig. 1), with measurements of the channel width made every 1000 m down flow. Eight lava flows were mapped on Arsia Mons (AM), Ascraeus Mons (AsM), and Pavonis Mons (PM) (Fig. 2). Mars Orbiting Laser Altimeter (MOLA) Precision Experimental Data Record (PEDR) (~160 m spot size, ~300 m along track spacing and 37 cm effective vertical resolution) data were also used to calculate the thickness of the flow. Slopes were then calculated utilizing the MOLA/High Resolution Stereo Camera (HRSC) (~200 m/pixel; ± 3 m vertical resolution) blended Digital Elevation Model (DEM) [11], and a slope transect was taken adjacent to each flow. Results for each flow are shown in Tables 1-2. All data analysis was performed in JMars and ArcGIS Pro.

Modeling Approach: Modeling of each lava flow follows the standard rheologic approach [5]. We outline the equations used in this modeling approach below.

Calculations: The measured values from Table 1 were used to calculate the effusion rate, viscosity, and yield strength of each lava flow. The Graetz number (G_z) equation is used to first calculate effusion rate:

$$G_z = Q/(kx)(hw) \quad (1)$$

The Jeffrey's equation is next used to calculate the effective dynamic viscosity with the effusion rate (Q) calculated in eq. (1):

$$\eta = \rho g h^3 w \sin(\alpha)/3Q \quad (2)$$

Yield strength (T) is defined as:

$$T = \rho g \sin(\alpha) h \quad (3)$$

Constants used throughout these equations include: k, the thermal diffusivity (5 x 10^{-7} m^2/s); the Graetz number (300); ρ, the lava density (2700 kg/m^3); and g, gravitational acceleration (3.7 m/s^2). The variables for each flow are the slope (a), average central channel width (w), flow thickness (h), and flow length (x).

Results: The results using the standard modeling approach for each lava flow with the average, minimum, and maximum slopes are found in Table 2.

The slope does not factor into the Graetz equation, hence the effusion rate for each flow remained constant. The viscosity calculations for the average slopes ranged from 1.24 x 10^7 to 5.17 x 10^{10} (Pa s) and for the minimum and maximum slopes, the viscosity varied from 7.72 x 10^4 to 5.58 x 10^{10} (Pa s) across all eight flows. The yield strength ranged from 2.02 x 10^4 to 2.8 x 10^5 (Pa), whereas the minimum and maximum slope value calculations varied from 2.89 x 10^3 to 4.02 x 10^5 (Pa). Using the average slope produced values that were generally about 80-90% higher than the values generated by the minimum slope.

Future Work: The work has focused on assessing how using minimum and maximum slope values impact the calculations; however, further analyses are planned.

Additional Calculations. In addition to using the minimum and maximum slope values, we will also utilize the minimum and maximum channel width in the calculations. These data will be compared to the data in Table 2. The variations will be analyzed to understand the differences and the sensitivity of the standard rheologic approach model to these inputs.

Comparison to prior studies. Four lava flows in this study were examined in prior studies [e.g., 6]. These are AM3, AsM2, AsM4, and PM1. The calculated effusion rate, viscosity, and yield strength data from each of these flows will be compared. The intent is to verify calculations here using those previous results.

Quantifying the topographic variability using linear regression. A method has been developed for quantifying the variability in Martian topography that utilizes simple linear regression [e.g., 9]. The topographic variability is closely correlated with the center of volcanic flows, and thus could provide additional statistics regarding the slope data collected and how the topography varies along each volcanic flow and ultimately, the effect that could have on flow length [9].

Self-Replication and PyFLOWGO models. Our investigation measured channelized flows. Both, the self-replication [2] and PyFLOWGO [4,12] models are also applicable to the formation and emplacement of Martian channelized lava flows. These models account for more variables than the standard rheologic approach. We plan to compare the results from these models to our initial findings.

Acknowledgements: This undergraduate student work was supported by NASA Solar System Workings (SSW) grant 80NSSC19K0547 to MSR.

References: [1] Mounginis-Mark P. J. & Glaze L S. (2003) *JGR: Planets, 108, 5066.* [2] Baloga S. M. & Glaze L. S. (2008) *JGR: Planets, 113.* [3] Garry W. B. et al. (2007) *JGR: Planets, 112.* [4] Flynn I. T. W. & Ramsey M. S. (2020) *LPSC LI, Abstract #1676.* [5] Hiesinger H. et al. (2007) *JGR: Planets, 112.* [6] Peters S. I. et al. (2021) *JGR: Planets, 126.* [7] Bleacher J. E. et al. (2007) *JGR: Planets, 112.* [8] Glaze L. S. & Baloga S. M. (2009) *JGR: Planets, 114.* [9] Glaze L. S. & Baloga S. M. (2007) *LPSC XXXVIII, Abstract #1162.* [10] Flynn I. T. W. et al. (2021) *LPSC LI, Abstract #1305.* [11] Fergason R. L. et al. (2018) Astrogeology PDS Annex, USGS. [12] Rowland S. K. et al. (2004) *JGR: Planets, 109*, 1-16.

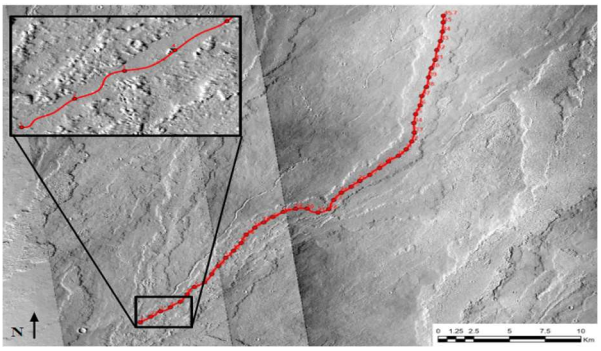

Figure 1: The AsM1 mapped lava flow located at 16.408°N, 260.884°E. Each flow was measured down the central channel, with data points every 1000 m (indicated by the red line and dots). Base map: CTX mosaic.

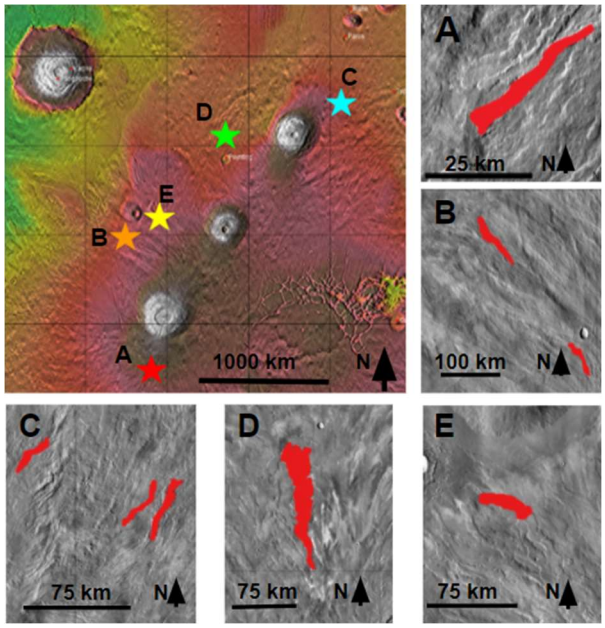

Figure 2: Location of the studied Tharsis lava flows. The colorized MOLA topography image has stars indicating the location of the inset CTX images. Inset A (AM1); B (AM2 and AM3); C (AsM1, AsM2, and AsM4); D (AsM3); and E (PM1).

Table 1: Measured values for the mapped lava flows in the Tharsis region

Name	Coordinates	Flow Length (km)	Avg. Central Channel Width (m)	Avg. Flow Width (m)	Avg. Flow Thickness (m)	Avg. Slope (°)
AM1	-16.996°N, 235.287°E	63.4	615	2690	26.8	0.45
AM2	-3.12°N, 239.621°E	39	696	2759	41	0.58
AM3	-1.076°N, 237.803°E	103	873	5777	27.4	0.44
AsM1	16.408°N, 260.884°E	44.7	622	2228	23	0.31
AsM2	15.611°N, 259.617°E	48.3	833	3577	13.4	0.99
AsM3	11.789°N, 245.426°E	172	2745	20548	47	0.64
AsM4	16.148°N, 261.492°E	81	1091	2881	20	0.64
PM1	1.355°N, 238.531°E	51	1514	6498	8.5	0.24

Table 2: Modeled values for the same mapped flows

Name	Avg. Slope (°)	Avg. Effusion Rate (m^3/s)	Avg. Viscosity (Pa s)	Avg. Yield Strength (Pa)	Min. Slope (°)	Min. Viscosity (Pa s)	Min. Yield Strength (Pa)	Max. Slope (°)	Max. Viscosity (Pa s)	Max. Yield Strength (Pa)
AM1	0.45	5.85×10^3	2.93×10^6	1.16×10^5	0.14	9.41×10^5	5.63×10^6	0.99	5.63×10^6	2.24×10^5
AM2	0.58	9.93×10^1	8.82×10^8	2.24×10^5	0.048	7.72×10^7	1.58×10^9	1.384	1.58×10^9	4.02×10^5
AM3	0.44	4.90×10^{-1}	5.17×10^{10}	$1.1\ 7x\ 10^5$	0.034	4.13×10^9	5.58×10^{10}	2.664	5.58×10^{10}	1.26×10^5
AsM1	0.31	1.81×10^2	4.24×10^7	7.01×10^4	0.034	4.72×10^6	9.22×10^7	0.725	9.22×10^7	1.52×10^5
AsM2	0.99	4.50×10^2	1.24×10^7	1.12×10^5	0.123	1.82×10^6	1.08×10^7	2.328	1.08×10^7	9.73×10^4
AsM3	0.64	1.51×10^3	2.76×10^9	2.80×10^5	0.034	2.14×10^7	5.01×10^8	4.061	5.01×10^8	3.73×10^5
AsM4	0.64	6.63×10^2	2.62×10^7	1.19×10^5	0.048	2.10×10^6	8.52×10^6	2.946	8.52×10^6	3.88×10^4
PM1	0.24	1.36×10^3	5.40×10^5	2.02×10^4	0.034	7.72×10^4	1.84×10^6	0.946	1.84×10^6	6.89×10^4